

## ARTICLE OPEN



# Deciphering the superior thermoelectric property of post-treatment-free PEDOT:PSS/IL hybrid by X-ray and neutron scattering characterization

Xin Li<sup>1</sup>, Ruike Zou<sup>1</sup>, Zhen Liu<sup>1</sup>, Jitendra Mata<sup>1,2</sup>, Ben Storer<sup>1,2</sup>, Yu Chen<sup>3</sup>, Weiheng Qi<sup>1,3,4</sup>, Zekun Zhou<sup>1</sup> and Peng Zhang<sup>1</sup>✉

In this work, a polymer and ionic liquid (IL) hybrid with superior thermoelectric performance is prepared via a system design of the chemical composition, molar ratio of the constituent molecules and manipulating the structure in solution and dried films. The solution-casted hybrid film, consisting of poly(3,4-ethylenedioxythiophene):poly(styrenesulfonate) (PEDOT:PSS) and 1-ethyl-3-methylimidazolium tricyanomethanide (EMIM:TCM), shows the highest power factor of  $175 \mu\text{W m}^{-1} \text{K}^{-2}$  in the polymer hybrid prepared by a post-treatment-free method. With a set of complementary structure characterization methods, it is found that EMIM:TCM can induce the structure reorganization of PEDOT:PSS in solution from a core-shell model to a rod-like model, during which PEDOT partially separates from PSS that eases the conductive network formation. In addition, the oxidation level of PEDOT:PSS is reduced by adding EMIM:TCM. Based on which, the PEDOT:PSS/IL hybrid shows the best performance in optimizing the conductivity ( $1163 \text{ S cm}^{-1}$ ) and Seebeck coefficient ( $38.8 \mu\text{V K}^{-1}$ ) simultaneously.

npj Flexible Electronics (2022)6:6; <https://doi.org/10.1038/s41528-022-00138-y>

## INTRODUCTION

Thermoelectric (TE) materials play an important role for the development of sustainable energy systems because it can generate electricity using the waste heat from factories, vehicles, mechanical devices, and even human bodies<sup>1,2</sup>. Recently, organic TE materials involving conductive polymer are under intensive research because of their unique features, including intrinsically low thermal conductivity, low cost, good mechanical flexibility, low or no toxicity, and good biocompatibility<sup>3</sup>. Moreover, their TE properties are highly tunable with rationally designed synthetic or fabrication methods, making them promising flexible TE materials for applications such as wearable and implantable electronics<sup>4,5</sup>. However, the performance of organic TE materials is generally much lower than that of the inorganic counterparts and generators, which limits their applications.

To improve the TE properties, plenty of organic TE materials have been developed in the last decades. Especially poly(3,4-ethylenedioxythiophene):poly(styrenesulfonate) (PEDOT:PSS), a complex of conducting PEDOT doped with insulating PSS, has attracted considerable research interest since its ease processability, good conductivity, and excellent biocompatibility. To further improve the conductivity, the wet-coated PEDOT:PSS usually needs pre- or post-treatments via secondary doping or solvent washing, to minimize the content of the isolating PSS components. Meanwhile, increasing the Seebeck coefficient values of the PEDOT:PSS is desired by referring to that the TE materials' properties are evaluated by a dimensionless figure-of-merit called  $ZT = S^2\sigma T/\kappa$ , where  $S$  ( $\mu\text{V K}^{-1}$ ) is the Seebeck coefficient,  $\sigma$  ( $\text{S cm}^{-1}$ ) is the electrical conductivity,  $T$  (K) stands for the absolute temperature, and  $\kappa$  ( $\text{W m}^{-1} \text{K}^{-1}$ ) represents the thermal conductivity<sup>6</sup>. In addition, considering the intrinsically low thermal

conductivity of PEDOT:PSS, a power factor ( $\text{PF} = S^2\sigma$ ) is used to evaluate their TE properties<sup>7,8</sup>.

To get a high PF value and good TE property, manipulating the molecular structure of PEDOT:PSS via hybridizing with inorganic (like Te- or C-based nanomaterials)<sup>9–13</sup> and organic components (such as organic solvent and ionic liquid)<sup>14–19</sup> have been generally reported. Especially, it is demonstrated that hybridizing with ionic liquids (ILs) could improve both the conductivity and Seebeck coefficient of the PEDOT:PSS simultaneously<sup>19,20</sup>. For example, Kee et al.<sup>19</sup> mixed PEDOT:PSS with 1-ethyl-3-methylimidazolium 4,5-dicyanoimidazolate (EMIM:DCl) and 1-ethyl-3-methylimidazolium dicyanamide (EMIM:DCA) in aqueous dispersion and prepared a stretchable PEDOT:PSS film with enhanced electrical conductivity and Seebeck coefficient (up to  $538 \text{ S cm}^{-1}$  and  $35 \mu\text{V K}^{-1}$ , respectively), comparing to the PEDOT:PSS film with  $\sigma \approx 1 \text{ S cm}^{-1}$  and  $S \approx 15 \mu\text{V K}^{-1}$ . The improved TE performance is ascribed to that ionic interaction between PEDOT:PSS and ILs promote microstructure reorganization and facilitates the formation of interconnected conductive PEDOT networks<sup>16,21–23</sup>.

To maximize the overall performance of the PEDOT:PSS-based TE materials, a complex process involving molecular design, solution structure and conductive network structure in the dried film manipulation recently has been taken into consideration. For example, Jang et al.<sup>24</sup> designed the molecular structure of IL, which hybridized with PEDOT:PSS to achieve a 5000-fold enhancement of conductivity (from 0.4 to  $2103 \text{ S cm}^{-1}$ ). Noteworthy, the hybridization occurred in solution via solution supramolecular assembly that endowed the dry film with a higher amount of  $\pi$ -stacked PEDOT aggregate. Pei's<sup>25</sup> and Chen's<sup>26</sup> groups have also found that the property of conjugate polymer film can be significantly improved via tuning the solution supramolecular assembly, which was studied by small angle

<sup>1</sup>State Key Laboratory of Optoelectronic Materials and Technologies, Key Laboratory for Polymeric Composite and Functional Materials of Ministry of Education, School of Materials Science and Engineering, Sun Yat-sen University, Guangzhou 510275, China. <sup>2</sup>Australian Centre for Neutron Scattering, Australian Nuclear Science and Technology Organisation, Lucas Heights, NSW 2234, Australia. <sup>3</sup>Beijing Synchrotron Radiation Facility, Institute of High Energy Physics, Chinese Academy of Sciences, Beijing 100049, China. <sup>4</sup>University of Chinese Academy of Sciences, Beijing 100049, China. ✉email: zhangpeng3@mail.sysu.edu.cn

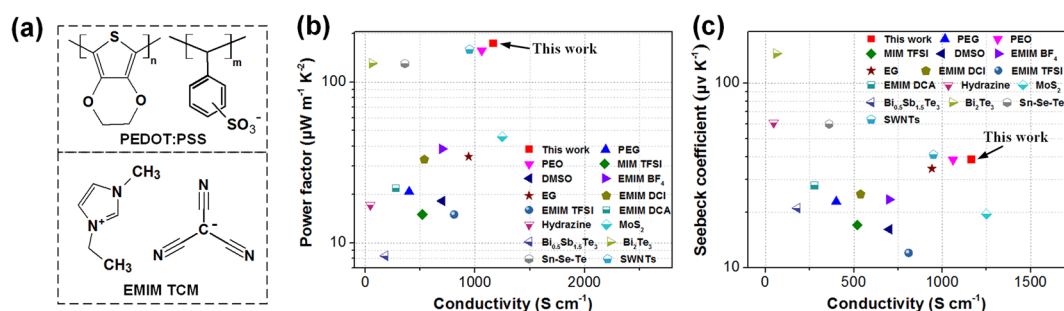


**Fig. 1** Chemical structures and TE performance of PEDOT:PSS. **a** Chemical structures of PEDOT:PSS and EMIM:TCM. **b, c** Comparison of the as-prepared PEDOT:PSS hybrid in this work with the reported post-treatment-free PEDOT:PSS at power factor (**b**) and Seebeck coefficient (**c**).

X-ray (SAXS) and neutron scattering (SANS)<sup>25</sup>. Recently, Ju et al.<sup>27</sup> attributed the improved TE property of doped PEDOT:PSS to the formation of an interconnected conductive network in the dried film, which was correlating to the structure change from initial core-shell structure of pristine PEDOT:PSS to the rod-like structure of doped PEDOT:PSS. In addition, plenty of other works have suggested that highly ordered microstructure<sup>28</sup> and conductive network in the dried film can ease the electron transfer for the enhancement of overall performance<sup>23,29</sup>. However, a systematic study of the structure-property correlation among additive molecular, solution structure, film structure, and TE property is still elusive, which brings obstacles for further improving the properties of the PEDOT:PSS-based TE materials.

In the present work, we hybridize the PEDOT:PSS with 1-ethyl-3-methylimidazolium tricyanomethanide (EMIM:TCM) via a system design including molar ratio of PEDOT:PSS and EMIM:TCM, the solution supramolecular assembly and conductive network in the dried film. Meanwhile, we want to focus on developing a simple and cost-efficient processing protocol, i.e., post-treatment free, which skips the cumbersome and sophisticated post-treatments and especially those with dangerous chemicals. We demonstrate a superior PF value of  $175 \mu\text{W m}^{-1} \text{K}^{-2}$ , which is, to the best of our knowledge, higher than the previous reported values in PEDOT:PSS-based post-treatment-free TE materials. A series of complementary characterization protocols have been undertaken to decipher the multiple-length scale structure from the molecular configuration to the long-range conductive network. We believe the post-treatment-free sample is a better model system to explore the correlation of the solution supramolecular assembly with the molecular packing in the dried film because the post-treatments usually would change the chemical composition of the dried film, for example. Our finding demonstrates that the TE performance of the PEDOT:PSS hybrid film could be further optimized via a system design of the material, shedding light on the large-scale production of post-treatment-free TE inks.

## RESULTS AND DISCUSSION

### TE property of the polymer hybrid

The TE materials were prepared by mixing the PEDOT:PSS with EMIM:TCM (Fig. 1a) in solution and then spin-coated into thin film. As shown in Fig. 1b, the PF of the spin-coated and post-treatment-free PEDOT:PSS/EMIM:TCM thin film is  $175 \mu\text{W m}^{-1} \text{K}^{-2}$  that is higher than the previously reported PEDOT:PSS hybrid with PEO<sup>14</sup>, ILs<sup>17,19</sup>, DMSO<sup>30</sup>, EG<sup>31</sup>, hydrazine<sup>32</sup> or inorganic TE fillers<sup>9,10,12,33,34</sup>. Notably, Saxena et al.<sup>20</sup> reported a high-record PF value of  $167 \mu\text{W m}^{-1} \text{K}^{-2}$  in PEDOT:PSS film through a post-treatment with EMIM:DCA and THF. By comparison, the as-prepared PEDOT:PSS/EMI:TCM film exhibits a better performance with PF of  $175 \mu\text{W m}^{-1} \text{K}^{-2}$  and electrical conductivity of  $1163 \text{ S cm}^{-1}$  (Fig. 1c). To the best of our knowledge, the present PF value is among the highest values of the post-treatment-free PEDOT:PSS hybrid thin films. In

addition, we should point out that the post-treatment even with simple water/ethanol washing could further enhance the TE performance, as demonstrated by Chen et al.<sup>35</sup>. However, the post-treatment and its influence on the materials' performance are out of the scope of the present work. In the following, we rationalize the superior TE properties of the as-prepared thin film from the perspective of system design, including molar ratio of IL, solution supramolecular assembly, hierarchical conductive network structure in the dried film.

### Solution structure study with SAXS and SANS

In the previous work, we have demonstrated that adding ILs or salts into PEDOT:PSS solution would disturb the charge interactions among PEDOT and PSS ions, and thus changes the supramolecular assembly of PEDOT:PSS in solution. Similar phenomenon relating to the solution supramolecular assembly have also been reported by Pei et al.<sup>25</sup> and Lu et al.<sup>36</sup>. To explore the structure of solution supramolecular assembly, small-angle X-ray scattering (SAXS) measurements, allowing structural analysis of flexible macromolecular systems<sup>37,38</sup>, were undertaken. As shown in Fig. 2b, neat PEDOT:PSS shows a shoulder peak at scattering vector  $q = 0.03 \text{ \AA}^{-1}$ , which diminishes with the increase of EMIM:TCM content. This phenomenon can be rationalized with the fact that adding IL has redirected the solution supramolecular assembly of PEDOT:PSS. To get solid information about the structural change, the SAXS data were fitted with a core-shell model<sup>39</sup> and rod-like model<sup>27</sup> (i.e., rigid PEDOT rod coupled with soft PSS Gaussian random coils) for PEDOT:PSS and PEDOT:PSS/EMIM:TCM (i.e., w/TCM), respectively. More detailed fitting results could be found in Supplementary Fig. 1 and Supplementary Note 1 of the Supplementary Information. The fitting results indicate that the connection of the conductive PEDOT changes from isolated spheres (Fig. 2a) to interconnected rod-like structures (Fig. 2c), which would ease the hole transfer in long-range. Our hypothesis is supported by the fact that the resistance value of the aqueous dispersions decreased from  $182 \text{ K}\Omega$  of PEDOT:PSS to  $1.14 \text{ K}\Omega$  of w/TCM 0.49 (cf. Supplementary Fig. 2 in the Supplementary Information). Similar results have been reported independently by Lee et al.<sup>23</sup> and Jang et al.<sup>24</sup>, who argued that IL changed electrostatic interactions and thus the supramolecular structure (including the  $\pi$ - $\pi$  stacking) of PEDOT:PSS. Following these findings mentioned above, we study the microstructure change before and after blending with IL with small-angle neutron scattering (SANS).

SANS is a well-established method for the characterization of polymer structure in solution by probing directly the temporal and spatial information of nanostructure or component selectivity via contrast matching<sup>40</sup>. SANS combined with SAXS could provide comprehensive structure information of PEDOT:PSS dispersion<sup>41</sup>. Different from the X-ray scattering relying on the electron density contrast, neutron scattering is based on the neutron-nuclei interactions and thus different isotopic species could give

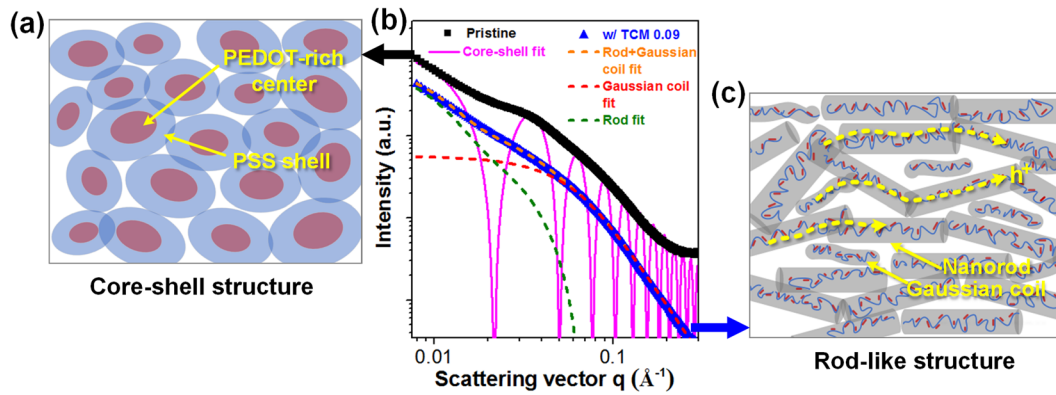


**Fig. 2 Solution supramolecular assembly of PEDOT:PSS solution.** **a, c** A microphase-segregated core (PEDOT)-shell (PSS) structure (**a**) and a rod-like microstructure (**c**) consisting of rigid rods and associated soft Gaussian coils, corresponding to PEDOT and PSS molecules, respectively, were used to fit the SAXS data of PEDOT:PSS hybrid solutions (**b**). The conductive pathway is schematically illustrated in (**c**) with dashed arrows.

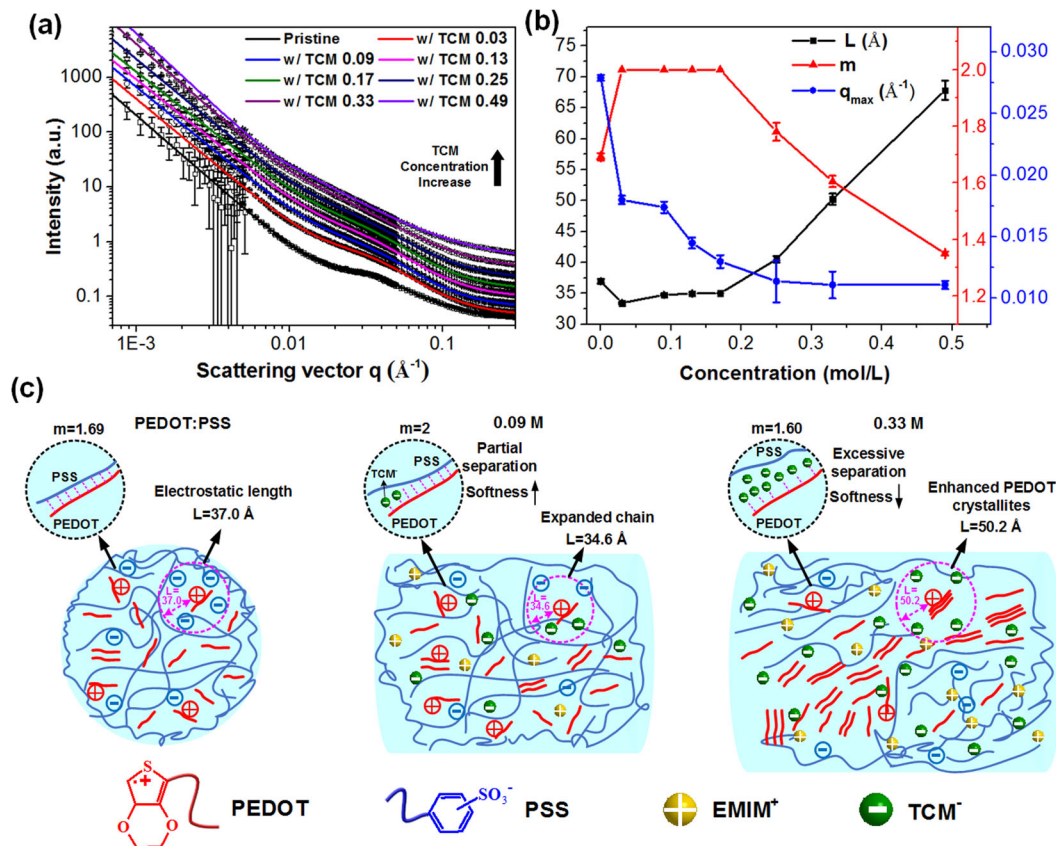


**Fig. 3 Solution microstructure of PEDOT:PSS solution.** **a** SANS results of PEDOT:PSS hybrid solutions as a function of the EMIM:TCM content, with deuterated water as the solvent. Hollow dots with error bar denote raw data and solid lines denote the fitted data with an empirical model. The error bars of the SANS curves are attributed to the intensity variation of the 2D scattering pattern during radial integration. **b** The extracted fitting parameter, indicating the structural change of PEDOT:PSS hybrid as a function of the EMIM:TCM content. Error bars indicate standard deviations. Note: some error bars are smaller than the plotting symbols. **c** Schematic illustration of the supramolecular assembly of PEDOT:PSS/EMIM:TCM hybrid in aqueous solution.

different SANS signal. For example, light hydrogen (H) has different neutron scattering length that leads to different signal magnitude and sign. Therefore, for the SANS experiments, the PEDOT:PSS sample was dispersed in deuterated water and more microstructure information about the impact of IL on the PEDOT:PSS supramolecular assembly is expected due to contrast enhancement. To interpret the physical insight of the SANS data

in Fig. 3a, we fit the data with a Broad Peak Model<sup>42</sup>, which is an empirical model often used to fit neutral and charged polymer systems that exhibit electrostatically driven correlation behavior. The model is defined as

$$I(q) = \frac{A}{q^n} + \frac{C}{1 + (|q - q_{\max}|L)^m} + B \quad (1)$$

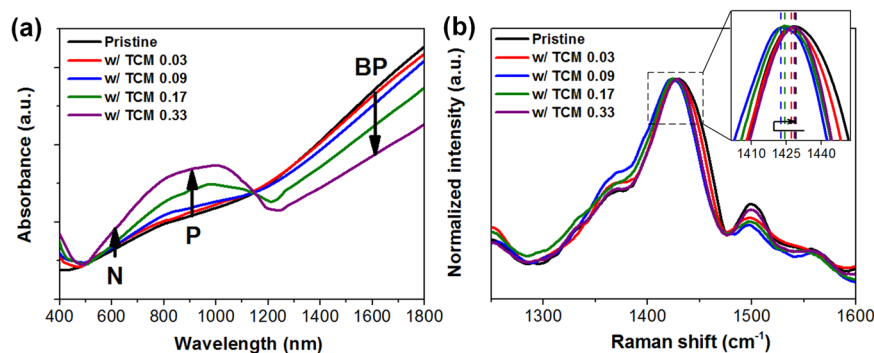


**Fig. 4 Molecular conformation of PEDOT:PSS hybrid film.** **a** UV–vis–NIR spectra and **b** Raman spectra of spin-coated PEDOT:PSS/EMIM:TCM hybrid thin films. Note that arrows marked with N, P and BP in **(a)** represent absorption features originating from neutral, polaronic and bipolaronic states, respectively. An inset consisting of details of the Raman peak shifts as a function of IL content is included in **(b)**.

where  $n$  is the low- $q$  scaling exponent;  $m$  is the high- $q$  scaling exponent,  $m$  reflects the stiffness of the polyelectrolyte chain, the higher the value, the softer of the chain;  $q_{\max}$  is the interchain correlation peak position;  $B$  is the background incoherent scattering and  $L$  is the electrostatic screening length of the interchain correlation. In addition, the  $L$  can be defined as the averaged distance between a charged segment and the surrounding segments with opposite charges. For example, pristine PEDOT:PSS (Supplementary Table 1) has an electrostatic correlation length  $L = 37.0$  Å. More details about the fitting results can be found in Supplementary Table 1 and Supplementary Note 2 of the Supplementary Information.

As shown in Fig. 3b,  $L$  values of the PEDOT:PSS/EMIM:TCM hybrid aqueous dispersion decreases first after mixing with a little of IL and then it increases gradually with the increase of IL content. A smaller  $L$  value corresponds to a shorter charge screening distance, which derives from the ionic exchange between PEDOT:PSS and EMIM:TCM, i.e., TCM anions replace the PSS to combine with the PEDOT, as demonstrated by previous reports<sup>23,24</sup>. The TCM anions have smaller volumetric occupation that could reduce the charge-dominated distance between adjacent PEDOT microdomains, i.e.,  $L$  value. However, the PEDOT chain conformation will be changed with the increase of IL content, resulting in the increase of  $L$  value. Similar phenomena have been demonstrated in the PEDOT:PSS hybrid with high-boiling-point solvent<sup>41</sup>. This conjecture can be rationalized by the fact that as EMIM:TCM concentration is increased,  $q_{\max}$  systematically decreases, which represents an increase in the screened correlation length ( $d = 2\pi/q$ ) among rigid charged PEDOT chains. The changes in polyelectrolyte chains' conformation can be further demonstrated by the parameter  $m$  and  $n$ .  $m$  value gets to the maximum (i.e.,  $m = 2$ ) and  $n$  gets to the minimum (cf. Supplementary Fig. 3 and Supplementary Note 3) when mixing a few EMIM:TCM (0.03–0.17 M) with PEDOT:PSS, indicating the PEDOT:PSS chains are in similar conformation with that in theta condition<sup>42</sup>. Further increase of the IL content (i.e., 0.25 M to 0.49 M) disturbs the system balance, indicated by both sharp decrease of  $m$  value and increase of  $n$  value, since PEDOT chains agglomerated to form rod-like structure as discussed above. Accordingly, the resistance of the w/TCM hybrid solution decreases (cf. Supplementary Fig. 2) which means a new conductive path formed already via IL-induced structural reorganization and solution supramolecular assembly. Schematic illustrations of solution structures are demonstrated in Fig. 3c and Supplementary Fig. 4. We anticipate that the IL-induced change of solution supramolecular assembly would have strong impact on the film structures and thus the TE properties of PEDOT:PSS/IL hybrid.

#### Dried thin film study with UV–vis, Raman, and GIWAXS

To prove our hypothesis, we characterized the molecular conformation and crystalline structure of the spin-coated PEDOT:PSS/EMIM:TCM hybrid film with UV–vis–NIR spectroscopy, Raman spectroscopy and grazing-incidence wide-angle X-ray scattering (GIWAXS) with synchrotron light. It's generally accepted that the oxidation level of PEDOT plays vital roles in the TE property, for example, the higher the oxidation level the lower is the Seebeck coefficient<sup>18,20</sup>. In the following, we improved the  $S$  value of PEDOT by manipulating the molar ratio of PEDOT:PSS and EMIM:TCM. To achieve that goal, we characterized the oxidation level of PEDOT with UV–vis–NIR spectroscopy (Fig. 4a and Supplementary Fig. 5a). By referring to the literature, the signal resulting from  $\pi-\pi^*$  transition of neutral PEDOT and from the polaron, bipolaron states along the PEDOT chains are marked with arrows at around 600, 900 and above 1250 nm, respectively<sup>18,43,44</sup>. By comparison, the signal intensity above 1250 nm decreases with the increase of IL content, opposite to the signal change at 600 and 900 nm, indicating that the mixing with IL has reduced the oxidation level of PEDOT. This conclusion was confirmed by the Raman spectroscopy result, as shown in Fig. 4b. IL hybridization narrows the width of the Raman peak centered at  $1429\text{ cm}^{-1}$ , which is assigned to the symmetric  $C_{\alpha}=C_{\beta}$  stretching vibrations of PEDOT rings<sup>45,46</sup>. This phenomenon indicates a dedoping of PEDOT<sup>27</sup>, agreeing well with the previous reports on reducing PEDOT with hydrazine<sup>47,48</sup>.

Raman spectra show the molecular conformation in PEDOT that plays vital role in the electron conductivity. The Raman peak at  $1429\text{ cm}^{-1}$  was used to judge the influence of IL on the PEDOT molecular conformation. For example, a red shifting of the peak signal is found when the IL concentration increases to 0.09 M, indicating the EDOT conformation changes from an original benzoid structure with favorite coil conformation to a quinoid structure with a favorite linear or expanded-coil structure<sup>43,49,50</sup>. Moreover, the quinoid structure endows PEDOT high planarity and eases the stacking of PEDOT chains, leading to fast charge transport. However, further increase of the IL content incurs the conformation transition from quinoid to benzoid structure, as indicated by the shifting of symmetric  $C_{\alpha}=C_{\beta}$  stretching vibration peak shown in the inset of Fig. 4b and Supplementary Fig. 5b. It's supposed that the sharp reduction in the oxidation level of PEDOT (Fig. 4a) localizes the charge along the PEDOT backbone and thus reducing the proportion of quinoid structure<sup>51,52</sup>.

To get more detailed information about the packing of PEDOT chains, we characterized the film structure with GIWAXS, which is a well-established protocol to characterize the molecular and crystalline structure of polymer at surface and beneath layers<sup>53–55</sup>. Figure 5a shows the typical 2D GIWAXS patterns that have been corrected for the “missing wedge” of data along the out-of-plane direction, a complete set of 2D pattern can be found in Supplementary Fig. 6 of the Supplementary Material. To interpret

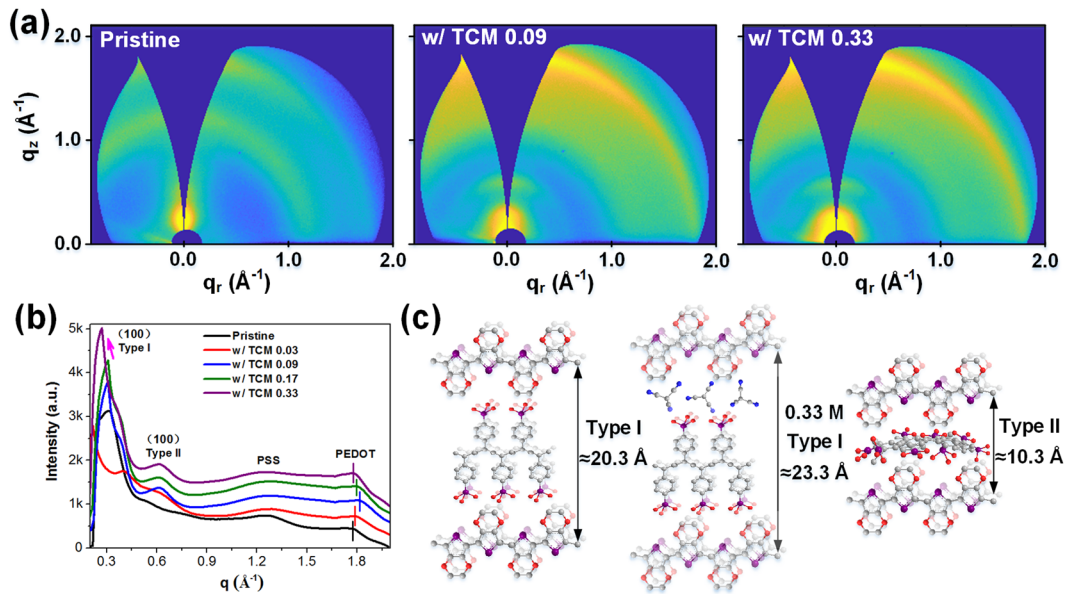


**Fig. 5 Crystalline structure of PEDOT:PSS hybrid film.** **a** Typical 2D GIWAXS patterns of PEDOT:PSS/EMIM:TCM hybrid films. **b** 1D GIWAXS scattering profiles integrated along cake cuts of the 2D patterns. **c** Schematic diagram of the lamellar stacking structures of PEDOT:PSS, extracted from the GIWAXS data analysis.

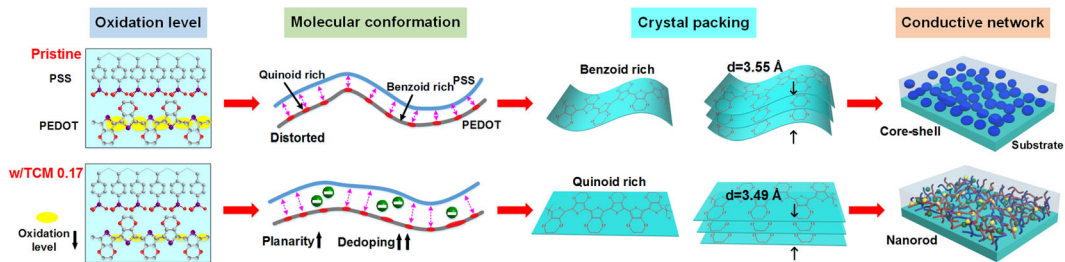


**Fig. 6 Multi-length scale structure of PEDOT:PSS.** Schematic diagram of multi-length scale structure of the pristine and IL-mixed PEDOT:PSS films.

the structure change, the 2D patterns were converted into 1D curves as shown in Fig. 5b. There are three characteristic peaks with  $q = 0.31 \text{ \AA}^{-1}$  ( $d = 20.27 \text{ \AA}$  calculated with  $d = 2\pi/q$ ),  $1.26 \text{ \AA}^{-1}$  ( $d = 4.99 \text{ \AA}$ ), and  $1.77 \text{ \AA}^{-1}$  ( $d = 3.55 \text{ \AA}$ ), which are attributed to alternating stacking of PEDOT and PSS (i.e., type I in Fig. 5c), the amorphous halo of PSS and  $\pi$ - $\pi$  stacking of PEDOT, respectively<sup>23,56</sup>. The peak position of the PEDOT (100) plane changes from  $q = 0.31 \text{ \AA}^{-1}$  (neat PEDOT:PSS) through  $q = 0.40 \text{ \AA}^{-1}$  (w/TCM 0.03,  $d = 15.71 \text{ \AA}$ ) to  $q = 0.27 \text{ \AA}^{-1}$  (w/TCM 0.33,  $d = 23.27 \text{ \AA}$ ), implying that a proper IL mixing brings a dense layer packing of PEDOT and PSS and an excess of IL content leads to the opposite result, which is schematically illustrated in Fig. 5c. One sharp peak appears at  $q = 0.61 \text{ \AA}^{-1}$  ( $d = 10.30 \text{ \AA}$ ) when the IL concentration is further increased, which is ascribed to a new type of layer stacking with alternating PEDOT and PSS chains (type II in Fig. 5c)<sup>29,57,58</sup>. Therefore, the type I and type II layer packing of PEDOT chains determine the conductive network in dried PEDOT:PSS hybrid film. The smaller is the layer spacing, the easier is the charge transport among adjacent conjugated chains<sup>59</sup>. By comparison with the type I, the type II layer packing eases the charge transport among adjacent PEDOT chains that means improved electron conductivity.

### Structure-property correlation analysis

$\pi$ - $\pi$  stacking of PEDOT is another important part of conductive network in PEDOT:PSS hybrid film. We investigate the impact of IL mixing on the  $\pi$ - $\pi$  stacking of PEDOT based on the GIWAXS data.

As marked in Fig. 5b, the peak position increases first from  $1.77 \text{ \AA}^{-1}$  (neat PEDOT:PSS) through  $1.79 \text{ \AA}^{-1}$  (w/TCM 0.03) to  $1.82 \text{ \AA}^{-1}$  (w/TCM 0.09) and decreases to  $1.78 \text{ \AA}^{-1}$  (w/TCM 0.33) through  $1.80 \text{ \AA}^{-1}$  (w/TCM 0.17). Correspondingly, the  $\pi$ - $\pi$  stacking distance ( $d = 2\pi/q$ ) decreases from  $3.55 \text{ \AA}$  (neat PEDOT:PSS) through  $3.51 \text{ \AA}$  (w/TCM 0.03) to  $3.45 \text{ \AA}$  (w/TCM 0.09) and then increases to  $3.53 \text{ \AA}$  (w/TCM 0.33) through  $3.49 \text{ \AA}$  (w/TCM 0.17). The detailed values of  $q$  and  $d$ -spacing are shown in Supplementary Table 2. A decrease in the  $\pi$ - $\pi$  stacking distance increases exponentially the  $\pi$ -electronic overlap and thereby enhances the effective movement of charge carriers<sup>27,60,61</sup>. This changed crystal stacking through mixing with IL is consistent with the previous reports<sup>20,23,27,56,58</sup>. By referring to the Raman spectroscopy results as mentioned above, we can have an in-depth understanding of the IL mixing induced structure change in PEDOT:PSS hybrid film. The planar quinoid structure helps the adjacent PEDOT chains form dense  $\pi$ - $\pi$  stacking; vice versa for the benzoid structure. Therefore, as schematically illustrated in Fig. 6, the best TE property could be achieved via balance of electric and thermo-electrical properties, i.e., hierarchical structure consisting of oxidation level, molecular conformation, crystal packing and conductive network. It's expected that the TE property indicated by  $PF = S^2\sigma$  should reach a maximum at a medium IL concentration, by balancing the TE and electric conductivities. For example, the w/TCM 0.17 achieves the best performance in optimizing the electrical conductivity ( $1163 \text{ S cm}^{-1}$ ) and Seebeck coefficient ( $38.8 \text{ \mu V K}^{-1}$ ) simultaneously.

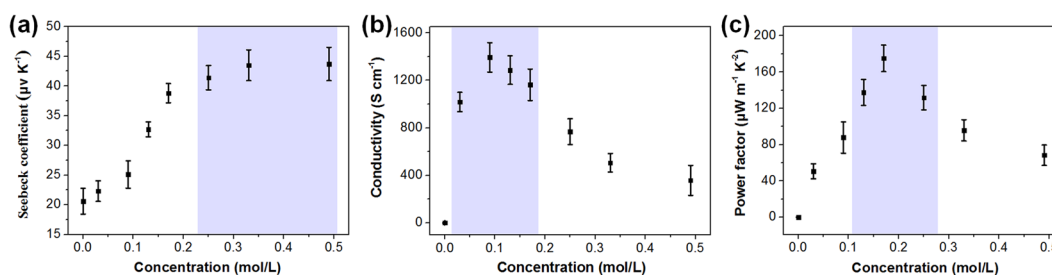


**Fig. 7 TE property of PEDOT:PSS/IL hybrid.** TE property of PEDOT:PSS hybrid film as a function of the EMIM:TCM content (a) Seebeck coefficient, (b) electrical conductivity and (c) power factor. Error bars represent standard deviation with at least five times measurement and it should be noted that some error bars are smaller than the plotting symbols.

To verify our hypothesis, we did a systematic study of the TE property of PEDOT:PSS hybrid film with different IL content. As shown in Fig. 7a, the Seebeck coefficient of the hybrid film increases monotonically with the increase of the EMIM:TCM content, which comes from a decrease in the oxidation level of PEDOT. In contrast, as shown in Fig. 7b, the electric conductivity of the hybrid film reaches a peak value (i.e.,  $1393 \text{ S cm}^{-1}$ ) at w/TCM 0.09, which could be rationalized by the formation of the complex hierarchical structure from oxidation level of PEDOT to conductive network of PEDOT as mentioned above. By comparison, the PF value of w/TCM 0.09 ( $88 \mu\text{W m}^{-1} \text{K}^{-2}$ , Fig. 7c and Supplementary Table 3) with  $S = 25.1 \mu\text{V K}^{-1}$ ,  $\sigma = 1393 \text{ S cm}^{-1}$  and  $\text{PF} = S^2\sigma$  is lower than that of w/TCM 0.17 ( $175 \mu\text{W m}^{-1} \text{K}^{-2}$ ) with  $S = 38.8 \mu\text{V K}^{-1}$  and  $\sigma = 1163 \text{ S cm}^{-1}$ . Furthermore, the PF value of w/TCM 0.17 sample shows much better (84% retention after 10 days, see Supplementary Fig. 7 and Supplementary Note 4 of the Supplementary Materials) environmental stability than that of pristine PEDOT:PSS (i.e., 59% retention). Our findings are expected to lay a way to improve the materials' property via manipulating the molecular assembly and structure design, which would promote the application of organic TE devices.

In this work, we demonstrate the successful preparation of a PEDOT:PSS/EMIM:TCM hybrid with superior TE property, i.e., PF value of  $175 \mu\text{W m}^{-1} \text{K}^{-2}$ , the conductivity of  $1163 \text{ S cm}^{-1}$  and Seebeck coefficient of  $38.8 \text{ mV K}^{-1}$ , by a post-treatment-free method. For one side, the post-treatment-free TE material is expected to be easily adapted to the industrial scale production process via slot-die coating, spray coating or roll to roll printing, promoting the commercialization of PEDOT-based flexible TEs. For the other side, it serves as a model system to explore the correlation of the solution supramolecular assembly with the molecular packing in the dried film without disturbing of the chemical composition and so on induced by post-treatments. After a systematic study based on a series of complementary characterization protocols, i.e., SAXS, SANS, UV-vis-NIR, Raman spectra and GIWAXS, the superior TE property of PEDOT:PSS/EMIM:TCM hybrid is attributed to the art of system design including molar ratio of PEDOT:PSS and EMIM:TCM, the solution supramolecular assembly and conductive network in the dried film. These fundamental knowledge would help the design and preparation of PEDOT:PSS hybrids with superior TE property and promote their applications in the fast-growing flexible and wearable device market.

## METHODS

### Sample preparation

PEDOT:PSS solid pellets (Orgacon Dry, Agfa Gevaert N.V., Belgium) were mixed with deionized (DI) water to form 1.3 wt% PEDOT:PSS aqueous dispersions after stirring. Afterwards, 1-ethyl-3-methylimidazolium tricyanomethanide (EMIM:TCM, TCI Chemical Industry Development Co., Ltd, Shanghai, China) was added to 1 mL of PEDOT:PSS aqueous to get the PEDOT:PSS/IL hybrid solution with molar concentration of IL varying from 0.03 to 0.49 M, and then vigorously stirred at room temperature overnight

(denoted as w/TCM X, X is the molar content of EMIM:TCM in the solution). NOTE: Heavy water (purity: 99.9%, Aladdin) replaced the normal water to prepare the samples for neutron scattering measurements. The glass substrates (24 mm × 24 mm) were sequentially treated with a detergent solution; sonicated in deionized water, acetone, and ethanol for 10 min each. To prepare the film samples, the as-prepared PEDOT:PSS hybrid solution were spread at 400 rpm for 18 s and then spin-coated onto glass substrates at 1000 rpm for 60 s under ambient conditions. Afterwards the film was dried in oven at  $50^\circ\text{C}$  for 30 min.

### Characterization

Seebeck coefficient measurements were undertaken at room temperature in the air with a home-made Peltier heater to control the sample temperature and a *Fluke Multimeter 8846A* to collect the thermovoltage. Seebeck coefficient value was estimated from the slope of the linear relationship between TE voltage and the temperature gap of the two probes. The measurements were performed by applying conductive silver paste to the samples at intervals of 6 mm and the diameter of the silver paste spot was around 1 mm (cf. Supplementary Fig. 8). Especially the Seebeck coefficient value was taken after 8 min balancing, to make sure that it was collected in a steady-state. The electrical conductivity was measured with a digital multimeter (RTS-8, Guangzhou Four Probe Technology Co., Ltd.) by following the four-probe method. The relative humidity was  $\sim 44\%$  during the conductivity and Seebeck coefficient measurements and the film thickness values were determined with a profilometer (Ambios XP-1, USA). The oxidation levels of the samples were characterized with an Ultraviolet–visible (UV–vis) absorption spectrometer (SHI-MADZU UV-3600 spectrophotometer) and an Ultraviolet–visible–near infrared (UV–vis–NIR) absorption spectrometer (Lambda 950 spectrometer, Perkin-Elmer). The Raman spectra of the films were obtained with a Raman spectrometer (Xplo RA Plus, HORIBA), equipped with a solid-state laser, excitation wavelength of 532 nm and diffraction grating 600/600. SANS data were obtained with the Quokka small-angle diffractometer at the Australian Nuclear Science and Technology Organization (ANSTO, Sydney). The solution sample was held in Hellma quartz cuvette cell for the SANS measurements<sup>52</sup>. The wavelength of the neutron was from 5 to 8.1 Å and the sample to detector distance was 1.3, 12, and 20 m. The fitting of SANS data after background subtraction was performed with a software package in the Igor Pro platform. SAXS experiments were performed with wavelength of 0.888 Å and the sample to detector distance (SDD) was 2756 mm, equipped with a Pilatus 1 M detector, and carried out at the BL19U2 station of Shanghai Synchrotron Radiation Facility (SSRF, China). Grazing-incidence wide-angle X-ray scattering (GIWAXS) with synchrotron light experiments were carried out at the 1W1A station of Beijing Synchrotron Radiation Facility (BSRF, China). The experiments were undertaken with a Huber 5-circle diffractometer and the scattered signal was collected with a 2D image plate (MAR-345, US) at  $\lambda = 1.54 \text{ \AA}$ . The  $\alpha_s$  and SDD were set to  $0.5^\circ$  and 438 mm, respectively. The SDD value was calibrated with a silver benenate sample. The GIWAXS data were analyzed with Matlab-based software GIXSGUI with the scattering vector  $q = 4\pi/\lambda \sin(\theta)$ <sup>53</sup>. Cake cut of the 2D GIWAXS pattern was performed with the azimuthal range from  $-16^\circ$  to  $16^\circ$  (with  $0^\circ$  being the polar direction of the detector plane).

### DATA AVAILABILITY

The authors declare that the data supporting the findings of this study are available within the paper (and its supplementary information files). Data are available upon request.

Received: 17 September 2021; Accepted: 17 December 2021;  
Published online: 27 January 2022

## REFERENCES

- Petsagkourakis, I. et al. Thermoelectric materials and applications for energy harvesting power generation. *Sci. Technol. Adv. Mater.* **19**, 836–862 (2018).
- Zhang, Q., Sun, Y., Xu, W. & Zhu, D. Organic thermoelectric materials: emerging green energy materials converting heat to electricity directly and efficiently. *Adv. Mater.* **26**, 6829–6851 (2014).
- Siddique, A. R. M., Mahmud, S. & Van Heyst, B. A review of the state of the science on wearable thermoelectric power generators (TEGs) and their existing challenges. *Renew. Sust. Energy Rev.* **73**, 730–744 (2017).
- Wang, Y. et al. Flexible thermoelectric materials and generators: challenges and innovations. *Adv. Mater.* **31**, 1807916 (2019).
- Lee, W., Lee, S., Kim, H. & Kim, Y. Organic thermoelectric devices with PEDOT:PSS/ZnO hybrid composites. *Chem. Eng. J.* **415**, 128935 (2021).
- Bubnova, O., Berggren, M. & Crispin, X. Tuning the thermoelectric properties of conducting polymers in an electrochemical transistor. *J. Am. Chem. Soc.* **134**, 16456–16459 (2012).
- Saxena, N. et al. Morphology-function relationship of thermoelectric nano-composite films from PEDOT:PSS with silicon nanoparticles. *Adv. Electron. Mater.* **3**, 1700181 (2017).
- Liu, J. et al. Thermal conductivity and elastic constants of PEDOT:PSS with high electrical conductivity. *Macromolecules* **48**, 585–591 (2015).
- Bharti, M. et al. Boosting thermoelectric power factor of free-standing Poly (3, 4-ethylenedioxythiophene):polystyrenesulfonate films by incorporation of bismuth antimony telluride nanostructures. *J. Power Sources* **435**, 226758 (2019).
- Zhang, B., Sun, J., Katz, H., Fang, F. & Opila, R. Promising thermoelectric properties of commercial PEDOT:PSS materials and their Bi<sub>2</sub>Te<sub>3</sub> powder composites. *ACS Appl. Mater. Interfaces* **2**, 3170–3178 (2010).
- Moriarty, G. P. et al. Thermoelectric behavior of organic thin film nanocomposites. *J. Polym. Sci., Part B: Polym. Phys.* **51**, 119–123 (2013).
- Yu, C., Choi, K., Yin, L. & Grunlan, J. C. Light-weight flexible carbon nanotube based organic composites with large thermoelectric power factors. *ACS nano* **5**, 7885–7892 (2011).
- El-Shamy, A. G. The role of nitrogen-carbon dots (NC) nano-particles in enhancing thermoelectric power functions of PEDOT:PSS/Te nano-composite films. *Chem. Eng. J.* **417**, 129212 (2021).
- Yi, C. et al. Enhanced thermoelectric properties of poly (3, 4-ethylenedioxythiophene):poly (styrenesulfonate) by binary secondary dopants. *ACS Appl. Mater. Interfaces* **7**, 8984–8989 (2015).
- Park, H. et al. Enhanced thermoelectric properties of PEDOT:PSS nanofilms by a chemical dedoping process. *J. Mater. Chem. A* **2**, 6532–6539 (2014).
- Li, X. et al. Effects of cationic species in salts on the electrical conductivity of doped PEDOT:PSS films. *ACS Appl. Polym. Mater.* **3**, 98–103 (2021).
- Mazaheripour, A. et al. Tailoring the Seebeck coefficient of PEDOT:PSS by controlling ion stoichiometry in ionic liquid additives. *Chem. Mater.* **30**, 4816–4822 (2018).
- Saxena, N. et al. Facile Optimization of thermoelectric properties in PEDOT:PSS thin films through acido-base and redox dedoping using readily available salts. *ACS Appl. Energy Mater.* **1**, 336–342 (2018).
- Kee, S. et al. Highly stretchable and air-stable PEDOT:PSS/ionic liquid composites for efficient organic thermoelectrics. *Chem. Mater.* **31**, 3519–3526 (2019).
- Saxena, N. et al. Ionic liquids as post-treatment agents for simultaneous improvement of Seebeck coefficient and electrical conductivity in PEDOT:PSS Films. *ACS Appl. Mater. Interfaces* **11**, 8060–8071 (2019).
- Badre, C., Marquant, L., Alsayed, A. M. & Hough, L. A. Highly conductive poly (3,4-ethylenedioxythiophene):poly (styrenesulfonate) films using 1-ethyl-3-methylimidazolium tetracyanoborate ionic liquid. *Adv. Funct. Mater.* **22**, 2723–2727 (2012).
- Yue, W. et al. A highly stretchable, transparent, and conductive polymer. *Sci. Adv.* **3**, e1602076 (2017).
- Kee, S. et al. Controlling molecular ordering in aqueous conducting polymers using ionic liquids. *Adv. Mater.* **28**, 8625–8631 (2016).
- de Izarra, A., Park, S., Lee, J., Lansac, Y. & Jang, Y. H. Ionic liquid designed for PEDOT:PSS conductivity enhancement. *J. Am. Chem. Soc.* **140**, 5375–5384 (2018).
- Zheng, Y. Q. et al. Unraveling the solution-state supramolecular structures of donor-acceptor polymers and their influence on solid-state morphology and charge-transport properties. *Adv. Mater.* **29**, 1701072 (2017).
- Deng, L., Huang, X., Lv, H., Zhang, Y. & Chen, G. Unravelling the mechanism of processing protocols induced microstructure evolution on polymer thermoelectric performance. *Appl. Mater. Today* **22**, 100959 (2021).
- Ju, D., Kim, D., Yook, H., Han, J. W. & Cho, K. Controlling electrostatic interaction in PEDOT:PSS to overcome thermoelectric tradeoff relation. *Adv. Funct. Mater.* **29**, 1905590 (2019).
- Deng, L. & Chen, G. Recent progress in tuning polymer oriented microstructures for enhanced thermoelectric performance. *Nano Energy* **80**, 105448 (2021).
- Kim, N. et al. Highly conductive PEDOT:PSS nanofibrils induced by solution-processed crystallization. *Adv. Mater.* **26**, 2268–2272 (2014).
- Luo, J. et al. Enhancement of the thermoelectric properties of PEDOT:PSS thin films by post-treatment. *J. Mater. Chem. A* **1**, 7576–7583 (2013).
- Jeong, M. H. et al. Increasing the thermoelectric power factor of solvent-treated PEDOT:PSS thin films on PDMS by stretching. *J. Mater. Chem. A* **6**, 15621–15629 (2018).
- Lee, S. H., Park, H., Son, W., Choi, H. H. & Kim, J. H. Novel solution-processable, doped semiconductors for application in thermoelectric devices. *J. Mater. Chem. A* **2**, 13380–13387 (2014).
- Ju, H., Park, D., Kim, K. & Kim, J. Exfoliated Sn-Se-Te based nanosheets and their flexible thermoelectric composites with poly (3, 4-ethylenedioxythiophene):Poly (styrenesulfonate) fabricated by solution processing. *Org. Electron.* **71**, 131–135 (2019).
- Jiang, F. et al. Use of organic solvent-assisted exfoliated MoS<sub>2</sub> for optimizing the thermoelectric performance of flexible PEDOT:PSS thin films. *J. Mater. Chem. A* **4**, 5265–5273 (2016).
- Deng, W., Deng, L., Li, Z., Zhang, Y. & Chen, G. Synergistically boosting thermoelectric performance of PEDOT:PSS/SWCNT composites via the ion-exchange effect and promoting SWCNT dispersion by the ionic liquid. *ACS Appl. Mater. Interfaces* **13**, 12131–12140 (2021).
- Li, T. et al. Effect of solvent on the solution state of conjugated polymer P7DPF including single-chain to aggregated state structure formation, dynamic evolution, and related mechanisms. *Macromolecules* **53**, 4264–4273 (2020).
- Chu, B. & Hsiao, B. S. Small-angle X-ray scattering of polymers. *Chem. Rev.* **101**, 1727–1762 (2001).
- Bernadó, P., Mylonas, E., Petoukhov, M. V., Blackledge, M. & Svergun, D. I. Structural characterization of flexible proteins using small-angle X-ray scattering. *J. Am. Chem. Soc.* **129**, 5656–5664 (2007).
- Takano, T., Masunaga, H., Fujiwara, A., Okuzaki, H. & Sasaki, T. PEDOT nanocrystal in highly conductive PEDOT:PSS polymer films. *Macromolecules* **45**, 3859–3865 (2012).
- Wiener, C. G., Wang, C., Liu, Y., Weiss, R. & Vogt, B. D. Nanostructure evolution during relaxation from a large step strain in a supramolecular copolymer-based hydrogel: a SANS investigation. *Macromolecules* **50**, 1672–1680 (2017).
- Murphy, R. J. et al. Scattering studies on poly (3, 4-ethylenedioxythiophene)-polystyrenesulfonate in the presence of ionic liquids. *Macromolecules* **48**, 8989–8997 (2015).
- Hammouda, B. Probing nanoscale structures—the sans toolbox. *J. Res. Natl. Inst. Stand. Technol.* 1–717 (2008).
- Fan, Z., Li, P., Du, D. & Ouyang, J. Significantly enhanced thermoelectric properties of PEDOT:PSS films through sequential post-treatments with common acids and bases. *Adv. Energy Mater.* **7**, 1602116 (2017).
- Khan, Z. U. et al. Acido-basic control of the thermoelectric properties of poly (3, 4-ethylenedioxythiophene) tosylate (PEDOT-Tos) thin films. *J. Mater. Chem. C* **3**, 10616–10623 (2015).
- Ouyang, J., Chu, C. W., Chen, F. C., Xu, Q. & Yang, Y. High-conductivity poly (3, 4-ethylenedioxythiophene):poly (styrene sulfonate) film and its application in polymer optoelectronic devices. *Adv. Funct. Mater.* **15**, 203–208 (2005).
- Wang, C. et al. Enhancement of conductivity and thermoelectric property of PEDOT:PSS via acid doping and single post-treatment for flexible power generator. *Adv. Sustain. Syst.* **2**, 1800085 (2018).
- Lee, S. H. et al. Transparent and flexible organic semiconductor nanofilms with enhanced thermoelectric efficiency. *J. Mater. Chem. A* **2**, 7288–7294 (2014).
- Culebras, M., Gómez, C. & Cantarero, A. Enhanced thermoelectric performance of PEDOT with different counter-ions optimized by chemical reduction. *J. Mater. Chem. A* **2**, 10109–10115 (2014).
- Mengistie, D. A. et al. Enhanced thermoelectric performance of PEDOT:PSS flexible bulky papers by treatment with secondary dopants. *ACS Appl. Mater. Interfaces* **7**, 94–100 (2015).
- Li, Z. et al. Mechanically robust and flexible films of ionic liquid-modulated polymer thermoelectric composites. *Adv. Funct. Mater.* **31**, 2104836 (2021).
- Kim, E.-G. & Brédas, J.-L. Electronic evolution of poly (3, 4-ethylenedioxythiophene)(PEDOT): From the isolated chain to the pristine and heavily doped crystals. *J. Am. Chem. Soc.* **130**, 16880–16889 (2008).
- Shi, W., Zhao, T., Xi, J., Wang, D. & Shuai, Z. Unravelling doping effects on PEDOT at the molecular level: from geometry to thermoelectric transport properties. *J. Am. Chem. Soc.* **137**, 12929–12938 (2015).

53. Zhang, P., Rothkirch, A., Koch, M., Roth, S. & Kraus, T. Determination of the surface facets of gold nanorods in wet-coated thin films with grazing-incidence wide angle X-ray scattering. *Part Part Syst. Char* **36**, 1900323 (2019).
54. Müller-Buschbaum, P. The active layer morphology of organic solar cells probed with grazing incidence scattering techniques. *Adv. Mater.* **26**, 7692–7709 (2014).
55. Huang, X., Deng, L., Liu, F., Liu, Z. & Chen, G. Aggregate structure evolution induced by annealing and subsequent solvent post-treatment for thermoelectric property enhancement of PEDOT:PSS films. *Chem. Eng. J.* **417**, 129230 (2021).
56. Palumbiny, C. M. et al. The crystallization of PEDOT:PSS polymeric electrodes probed in situ during printing. *Adv. Mater.* **27**, 3391–3397 (2015).
57. Kim, N. et al. Role of interchain coupling in the metallic state of conducting polymers. *Phys. Rev. Lett.* **109**, 106405 (2012).
58. Bießmann, L. et al. Highly conducting, transparent PEDOT:PSS polymer electrodes from post-treatment with weak and strong acids. *Adv. Electron. Mater.* **5**, 1800654 (2019).
59. Lu, Y. et al. The critical role of dopant cations in electrical conductivity and thermoelectric performance of n-doped polymers. *J. Am. Chem. Soc.* **142**, 15340–15348 (2020).
60. Kim, H. G. et al. Synthetic tailoring of solid-state order in diketopyrrolopyrrole-based copolymers via intramolecular noncovalent interactions. *Chem. Mater.* **27**, 829–838 (2015).
61. Lu, Y. et al. Rigid coplanar polymers for stable n-type polymer thermoelectrics. *Angew. Chem.* **131**, 11512–11516 (2019).
62. Wood, K. et al. QUOKKA, the pinhole small-angle neutron scattering instrument at the OPAL Research Reactor, Australia: design, performance, operation and scientific highlights. *J. Appl. Crystallogr.* **51**, 294–314 (2018).
63. Zhang, P. et al. Preparation of long-range ordered nanostructures in semi-crystalline diblock copolymer thin films using micromolding. *Chin. J. Polym. Sci.* **32**, 1188–1198 (2014).

## ACKNOWLEDGEMENTS

The authors acknowledge the financial supports from the National Natural Science Foundation of China (No. 11905306 and U2032101), Fundamental Research Funds for the Central Universities (No. 19lgpy14), and “100 Top Talents Program” of Sun Yat-sen University. X-ray data were acquired at beamline 19U2, SSRF, China. Neutron scattering data were obtained at ANSTO, Sydney. The authors gratefully acknowledge the technical assistance of Dr. Guangfeng Liu of 19U2 beamline during the beamtime.

## AUTHOR CONTRIBUTIONS

P.Z. designed and supervised the project. X.L. performed the material preparation, characterization, and result discussion. R.Z. participated in the data analysis. Z.L. participated in material preparation and result discussion. J.M. and B.S. contributed to the SANS test and result discussion. Y.C. and W.Q. contributed to the GIWAXS test. Z.Z. contributed to TE test. X.L. and P.Z. wrote the paper. All authors provided comments for the manuscript.

## COMPETING INTERESTS

The authors declare no competing interests.

## ADDITIONAL INFORMATION

**Supplementary information** The online version contains supplementary material available at <https://doi.org/10.1038/s41528-022-00138-y>.

**Correspondence** and requests for materials should be addressed to Peng Zhang.

**Reprints and permission information** is available at <http://www.nature.com/reprints>

**Publisher's note** Springer Nature remains neutral with regard to jurisdictional claims in published maps and institutional affiliations.



**Open Access** This article is licensed under a Creative Commons Attribution 4.0 International License, which permits use, sharing, adaptation, distribution and reproduction in any medium or format, as long as you give appropriate credit to the original author(s) and the source, provide a link to the Creative Commons license, and indicate if changes were made. The images or other third party material in this article are included in the article's Creative Commons license, unless indicated otherwise in a credit line to the material. If material is not included in the article's Creative Commons license and your intended use is not permitted by statutory regulation or exceeds the permitted use, you will need to obtain permission directly from the copyright holder. To view a copy of this license, visit <http://creativecommons.org/licenses/by/4.0/>.

© The Author(s) 2022